Full paper

Photoinduced triboelectric polarity reversal and enhancement of a new metal/semiconductor triboelectric nanogenerator

Juanjuan Han[a,b,1], Xiude Yang[a,b,c,1], Liping Liao[a,b], Guangdong Zhou[a,b], Gang Wang[a,b], Cunyun Xu[a,b], Wei Hu[a,b], Mbeng Elisabeth Reine Debora[a,b], Qunliang Song[a,b,*]

[a] Institute for Clean Energy & Advanced Materials, Faculty of Materials and Energy, Southwest University, Chongqing 400715, PR China
[b] Chongqing Key Laboratory for Advanced Materials and Technologies of Clean Energy, Chongqing 400715, PR China
[c] School of Physics and Electronic Science, Zunyi Normal College, Zunyi 563002, PR China

ARTICLE INFO

ABSTRACT

We reported a novel metal/semiconductor triboelectric nanogenerator (TENG) based on Au and TiO_2 as the friction layers. Upon illumination, the current polarity rapidly reverses compared to the dark state. The negative and positive short-circuit current approximately increase by 12 and 2 times, respectively. Particularly, a photocurrent plateau appears due to the formation of metal-semiconductor Schottky contact in the device. By carefully analyzing the charge transfer in dark and under illumination, it is found that the accumulation of a large number of photoelectrons on the surface of TiO_2 and the increase of conductivity are the reasons for the reversal current polarity and significant current increase under illumination. Our work provides a new approach for improving TENG output and a new understanding about the effect of surface states on the triboelectric performance especially the polarity of TENG.

1. Introduction

Triboelectric nanogenerator (TENG) is a new type of energy collection device that was first reported in 2012 [1]. By converting the mechanical energy that is ubiquitous in the environment into electricity, TENG can power small electronic devices or serve as a self-powered nanosensor [2–5]. To a large extent, it can effectively save traditional non-renewable energy and ease the energy crisis. The working principle of TENG is based on the triboelectrification and electrostatic induction. The difference of the triboelectric polarity at two contact layers causes induced charges on the respective electrodes to flow through the external circuit. [6]. Therefore, any two different materials with obviously opposite triboelectric polarity can be used as the friction layers in TENG. There are a wide variety of materials to be chosen for TENG. Some organic materials are often used in metal/polymer system due to the strong triboelectrification, such as polydimethylsiloxane (PDMS) [7,8], polytetrafluoroethylene (PTFE) [9–11], Kapton, etc. [12]. In addition, some nanostructure materials are used as friction layers in semiconductor/polymer system TENG to increase the contact area, such as TiO_2 nanowires [13] and SiO_2 nanoparticles [14]. More importantly, it has been demonstrated that the output of the TENG can be changed due to excellent photoelectric

properties of semiconductor materials by incorporating solar energy [15,16]. In fact, both photoconductivity and surface charge density of a semiconductor material can be changed to modulate triboelectric polarity between two contact materials under illumination [17]. Su et al. reported a TENG with reduced output upon illumination because the photoinduced holes partially neutralize the negative triboelectric charges on the surface of organolead halide perovskite, resulting in a decrease in surface charge density [18]. At the same time, by adding the photoinduced holes onto the triboelectric positive charges to increase the surface charge density, Su et al. demonstrated a photoinduced enhancement of TENG based on organolead halide perovskite/PTFE interface [19]. In 2017, Ye et al. reported a photoinduced enhancement of TENG in an opposite direction, which was ascribed to the photoinduced electrons generated in the light absorbing layer which transport through the electronic transport layer and then accumulate at the surface of TiO_x layer. This TENG is based on TiO_x /polyimide as friction layers and has a very complex structure (Al/polyimide, TiO_x/ $P3HT:PC_{61}BM/PEDOT:PSS/ITO/glass$) by preparing functional layers with a variety of different materials [20].

In this paper, we designed a brand new and simple metal/semiconductor TENG based on the ultrathin Au film and TiO_2 layer as friction materials. Compared with the dark situation, the current
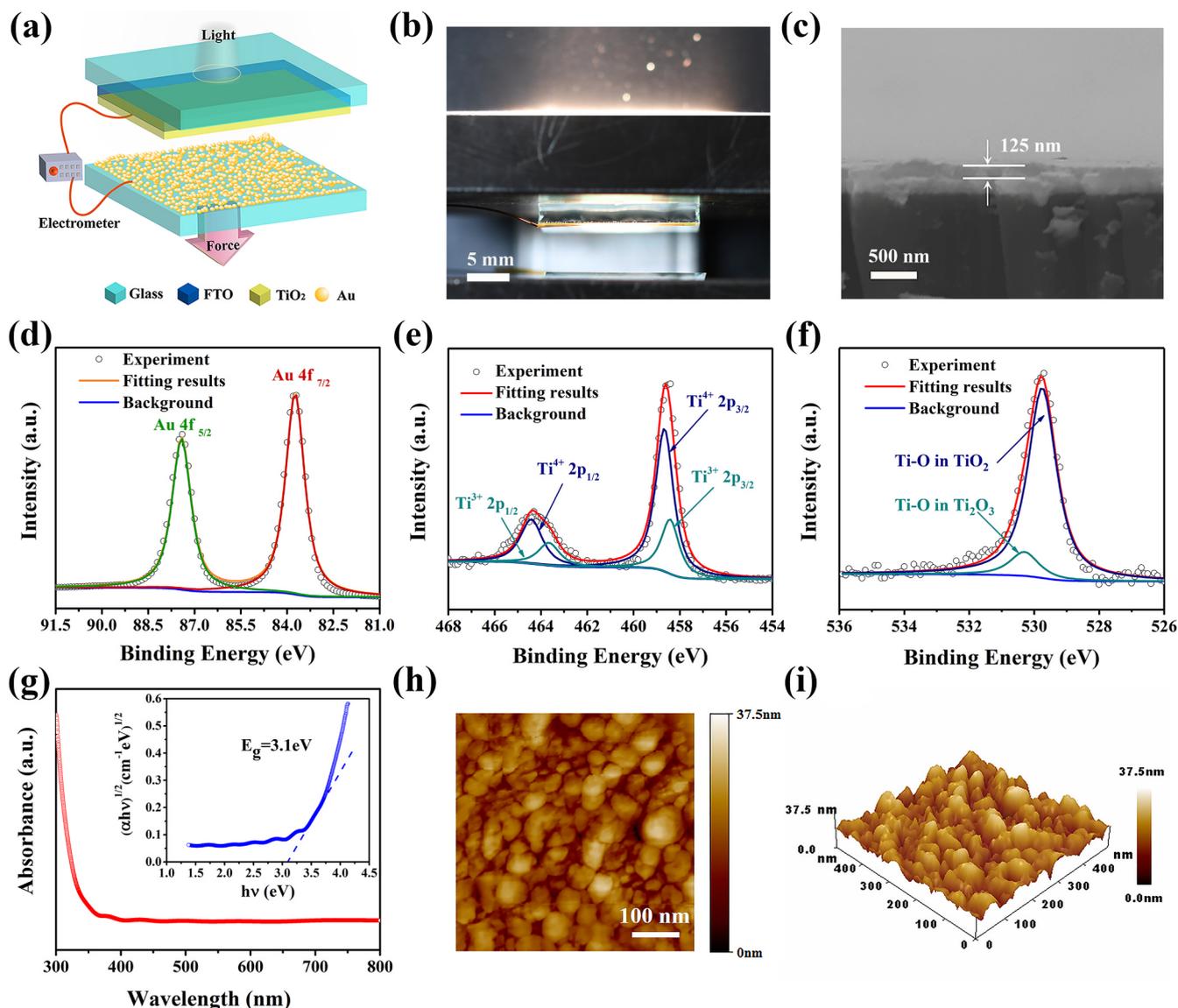

Fig. 1. The structure and characterization of the TENG. (a) The schematic diagram of the TENG under external vertical mechanical force and upon illumination. (b) The photograph of the fabricated TENG under illumination. (c) The cross-sectional FE-SEM image of the TiO_2 layer on the FTO glass. The XPS spectra of (d) Au 4f, (e) Ti 2p, (f) O 1s, respectively. (g) The UV absorbance spectrum of the TiO_2 and plot (inset) of $h\nu$ versus $(\alpha h\nu)^{1/2}$. (h) The AFM surface morphology images of TiO_2. (i) The AFM three-dimensional features of TiO_2.

polarity is reversed instantaneously upon illumination with 12 and 2 times increase for negative and positive short-circuit current, respectively. Moreover, the TENG can be transformed to a solar cell and generate a 5 nA photocurrent plateau due to the full physical contact of the metal and semiconductor. Our research broadens the understanding of a TENG made of metal and semiconductor rather than insulating polymers. The surface states play the key role in determining the magnitude and polarity of triboelectric current.

2. Experimental part

The schematic structure of the TENG is illustrated in Fig. 1a. The upper half of the device is simply the glass/FTO/TiO_2 and the lower half is the Au/glass. The process of the TENG fabrication is described as follows. Before preparing the ultrathin Au films and TiO_2 films, FTO (Fluoride doped SnO_2 on glass) substrates were immersed and sonicated in deionized water with detergent for 30 min followed by rinsing with deionized water then sonicated in ethanol, finally dried with the clean nitrogen flow. The precursor of TiO_2 was prepared by mixing a certain

percentage of hydrochloric acid (HCl) and 2-propanol (C_3H_8O) and stirring mechanically for 5 min, then Titanium (IV) isopropoxide ($C_{12}H_{28}O_4Ti$) was added into solution with strong stirring at room temperature to form a homogeneous precursor. The TiO_2 layers were fabricated by spin-coating the precursor solution onto the cleaned FTO glass substrate, then annealed in a muffle furnace at 450 °C in atmosphere for 30 min. The magnetic sputtering system was used to prepare the ultrathin Au film on the cleaned glass. The pressure in the vacuum was about 0.35 Pa. Argon was used as the working gas to deposit the thin film with power of 14 W for 50 s. Typically, we applied a layer of sponge tape as a buffer layer on the back of the glass substrate to ensure the complete contact between TiO_2 and Au. Finally, copper wires were connected with the FTO electrode and Au film to complete the device fabrication for data acquisition.

3. Characterization

The cross-section of the glass/FTO/TiO_2 was obtained by a field emission scanning electron microscopy (FE-SEM; JSM-7800F). Al Kα

with a pass energy of 30 eV was used in the X-ray photoelectron spectroscopy (XPS; ESCALAB 250Xi) to characterize the surface information of TiO$_2$ and Au film. An ultraviolet spectrometer (UV-2550) was used to analyze the absorption of the TiO$_2$ film. The surface morphology and roughness of the TiO$_2$ were characterized by scanning probe microscope system (CSPM5500). The thickness of the Au film was obtained by the dual rotating-compensator Mueller matrix ellipsometer (ME-L ellipsometer). The data of the TENG were collected by Keithley 6514 System Electrometer and a Data Acquisition Card (NI PCI-6259). The process of contacting and separating of the TENG was controlled by a linear motor (WMUA512075-06-D). Tungsten Halogen light source (CROWNTECH, CTTH -150W) was used to illuminate the device.

4. Results

Fig. 1a depicts the simple structure of the TENG device, which is composed of two parts. The upper TiO$_2$ layer serves not only as a triboelectrification layer but also as a light absorber. The lower ultrathin Au film acts not only as another friction layer but also as an electrode. The dimension of the device is $18 \times 18\,mm^2$ and the effective contact area is $14 \times 8\,mm^2$. The maximum separation distance (d) between the upper and lower parts is 2 mm. Light illumination on the TiO$_2$ is through a 10 mm diameter circular hole in the stator of the linear motor. Fig. 1b shows a photograph of a real TENG device under illumination. The upper and lower parts are respectively fixed onto the stator and motion module of the linear motor. The TiO$_2$ layer on FTO glass has a thickness of 125 nm, which was characterized by FE-SEM, as shown in Fig. 1c. The fitting thickness of Au film which was obtained by ME-L ellipsometer is about 6.2 nm. The Au film and TiO$_2$ layer were analyzed with XPS and the corresponding results are shown in Fig. 1d, e and f. The XPS data were calibrated with the carbon-carbon bond binding energy of 284.6 eV. The position of Au 4f$_{7/2}$ peak and Au 4f$_{5/2}$ are located at a binding energy of 83.7 and 87.4 eV, respectively, as shown in Fig. 1d, which are well agreed with previous reports, indicating that the Au film is in pure metallic form [21]. Fig. 1e shows symmetric Ti 2p peaks of Ti 2p$_{3/2}$ (~458.5 eV) and Ti 2p$_{1/2}$ (~464.2 eV). Both the spectral features and the values of binding energy are well consistent with the reported Ti^{4+} in TiO$_2$ lattice [22]. The binding energy difference of the spin-orbital splitting peaks is 5.7 eV, indicating that Ti^{4+} are abundant in oxidation states. Also, there are a few Ti^{3+} formed in the film corresponding to Ti$_2$O$_3$, indicating the nonstoichiometry of the titanium oxide [23]. The O1s spectrum of TiO$_2$ is shown in Fig. 1f. The core peaks are located at binding energies of 529.8 eV and 530.3 eV, which are Ti-O bond attributed to TiO$_2$ and Ti$_2$O$_3$, respectively. The UV absorbance spectrum of the TiO$_2$ reveals a strong absorption below 400 nm in Fig. 1g. In addition, the indirect optical band gap and absorption edge of the TiO$_2$ are calculated from Tauc plot in the inset, indicating that the optical bandgap E$_g$ of TiO$_2$ is ~3.1 eV [24]. Fig. 1h and i, respectively describe the surface morphology and three-dimensional features of TiO$_2$, revealing that TiO$_2$ is a compact film with an average surface roughness of 3.76 nm.

The performance of the TENG was characterized by measuring its short-circuit current (I$_{sc}$) and open-circuit voltage (V$_{oc}$), as shown in Fig. 2a and b. The upper and lower parts of the TENG are respectively fixed onto the stator and motion module of the linear motor. The motion of the motor causes periodic contact and separation between ultrathin Au film and TiO$_2$ layer. In dark condition, the average peak-to-peak values of the I$_{sc}$ and V$_{oc}$ are 7.5 nA and 0.36 V, respectively.

Fig. 3a depicts the change in current output of the TENG during the process of turning on and off light. In the dark state, the current signal is only from the periodically mechanical energy supplied by the linear motor, the average positive I$_{sc}$ and the negative I$_{sc}$ are only 5.4 and −2.1 nA, respectively. As a full-spectrum tungsten lamp is turned on, the average positive and negative I$_{sc}$ increase up to 16.7 and −28 nA, representing the enhancement up to approximately 2 and 12 times, respectively. Fig. 3b, c, and d are detailed enlarged plots. At the

moment of turning on the light source, the output current of TENG increases rapidly. It is worth noting here that the current immediately increases with the opposite direction. Additionally, there is a photocurrent plateau appeared when the ultrathin Au film and TiO$_2$ layer are in close contact in each cycle as shown in Fig. 3b. When the light illumination continues for a few seconds, the plateau current remains stable and reaches to 5 nA, as shown in Fig. 3c. When the light is turned off, the photocurrent plateau rapidly disappears, and the peak-to-peak current gradually decreases and recovers to the original dark state after about 1 min, which is shown in Fig. 3d.

5. Discussion

To investigate the surface triboelectric transfer charges mechanism and the behavior of photoelectrons, the contact-separation process of TENG is divided into two parts to discuss. When the distance d of the two friction surfaces is below the critical tunneling distance z [25], the electrons can move between both surfaces to maintain an equal Fermi level. When the distance is above z, the energy barrier of air is sufficiently high so that electron tunneling cannot occur. Therefore, oppositely charged surfaces of the two contact materials induce charges on the respective electrodes due to the triboelectrification and electrostatic induction. So there is a periodic alternating current signal formed in the external circuit to balance the potential difference during the contact-separation process.

Fig. 4 depicts the current signals of TENG 's two friction layers from tightly physical contact to completely separation in dark and upon illumination respectively. Since there are a lot of surface states at the surface of TiO$_2$ which can trap electrons, the surface Fermi level is pinned at the surface of TiO$_2$ and it is supposed to be higher than the Fermi level of Au. In the dark state, before contacting, few electrons have already been trapped on the surface of TiO$_2$. When TiO$_2$ and Au are fully contacted by mechanical force so that the d < z, the electrons on TiO$_2$ are transferred from the surface states to Au as exhibited in Fig. 4a. When TiO$_2$ and Au are separated by a mechanical force to lead d > z, the surface of TiO$_2$ would be positively charged since it has already lost electrons during contact. Further increasing the separation distance of TiO$_2$ and Au surfaces will increase the potential difference between them, driving the electrons flow from Au film to FTO electrode. So there is a positive current in the external circuit as described in Fig. 4b. While the approaching between TiO$_2$ and Au will decrease the potential difference between these two surfaces, driving electrons on FTO flow back to Au and generate the negative current.

The difference under illumination compared to dark condition is that the electrons on the valence band of TiO$_2$ are excited to generate a large number of electron-hole pairs. Before the physical contact between TiO$_2$ and Au, more electrons are trapped at those surface states due to the surface defects of TiO$_2$ [26]. Therefore, when the Au and TiO$_2$ are in full contact and d < z, due to that the surface Fermi level of TiO$_2$ is higher than that of Au, those electrons trapped on the surface states are efficiently transported from TiO$_2$ to Au to generate a positive photocurrent spike. After several cycles of contact separation, results in a stable photocurrent plateau of 5 nA. In fact, the structure of FTO/TiO$_2$/Au is working as a solar cell under this situation, as depicted as in Fig. 4d. While the distance increases and d > z, the photocurrent plateau disappears, leaving positive charges on the surface of TiO$_2$ due to equal number of electrons have been transferred to Au when TiO$_2$ is tightly touched with Au. However, during the process of increasing the separation distance, photoelectrons are continuously generated and accumulated on the surface of TiO$_2$. After completely neutralizing the positive charges, a lot of surplus photoelectrons trapped at those available surface states of TiO$_2$ make the surface negative. Therefore, the triboelectric polarity of TiO$_2$ is changed from positive in dark to negative under illumination, as shown in Fig. 4e. The number of electrons trapped on the TiO$_2$ surface under illumination is much larger than that of the positive charges left under dark condition. The short-
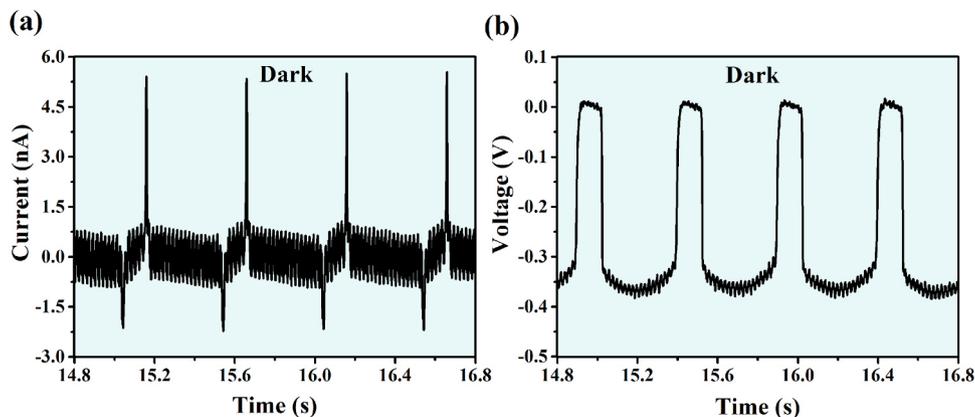
Fig. 2. The output of the TENG during a certain period of time in dark condition. (a)The I_{sc}, (b) the V_{oc} of the TENG at the frequency of 2 Hz.

circuit current changes direction rapidly and increase accordingly. Fig. 4c and f schematically show current polarity change during separation. The cyan and red curves represent positive and negative current in dark and under light irradiation, respectively.

After removing the light, the electrons on the TiO$_2$ are no longer excited and the photocurrent plateau disappears. The TENG's output current reverts to the dark situation after several cycles of contact-separation. This is because the electrons have been trapped by the surface states under illumination can only transfer some of them to Au at each contact. Similarly, the comparison of output voltage in dark and under illumination is shown in Fig. S1. As a full-spectrum tungsten lamp is turned on, the voltage of TENG immediately changes the direction. When the light is turned off, the voltage gradually decreases and recovers to the original dark state after about 1 min.

By using optical filter with wavelength below 400 nm, the output current is changed obviously. This means that the observed current improvement is mainly owing to the light below 400 nm. TiO$_2$ is an indirect semiconductor with a wide band gap of 3.1 eV as we have calculated before. The electrons are excited from the valence band to the conduction band and then trapped by the surface states that increases the surface electron density significantly. When using the light with wavelength in the range of 400–500 nm, there is a slightly increase in output which can be mainly attributed to the electrons directly transited from the valence band to the surface states [27], increasing the surface electron density of TiO$_2$ to some extent. The comparison of current output in dark and under illumination with different light wavelengths is shown in Fig. S2.

To further analyze the mechanism of TENG's current improvement upon light illumination, the conductive AFM under different applied bias voltages are compared in dark and under illumination. As shown in Fig. 5, the current under illumination is apparently higher than that in dark at -2 V bias voltage, indicating the enhancement of conductivity
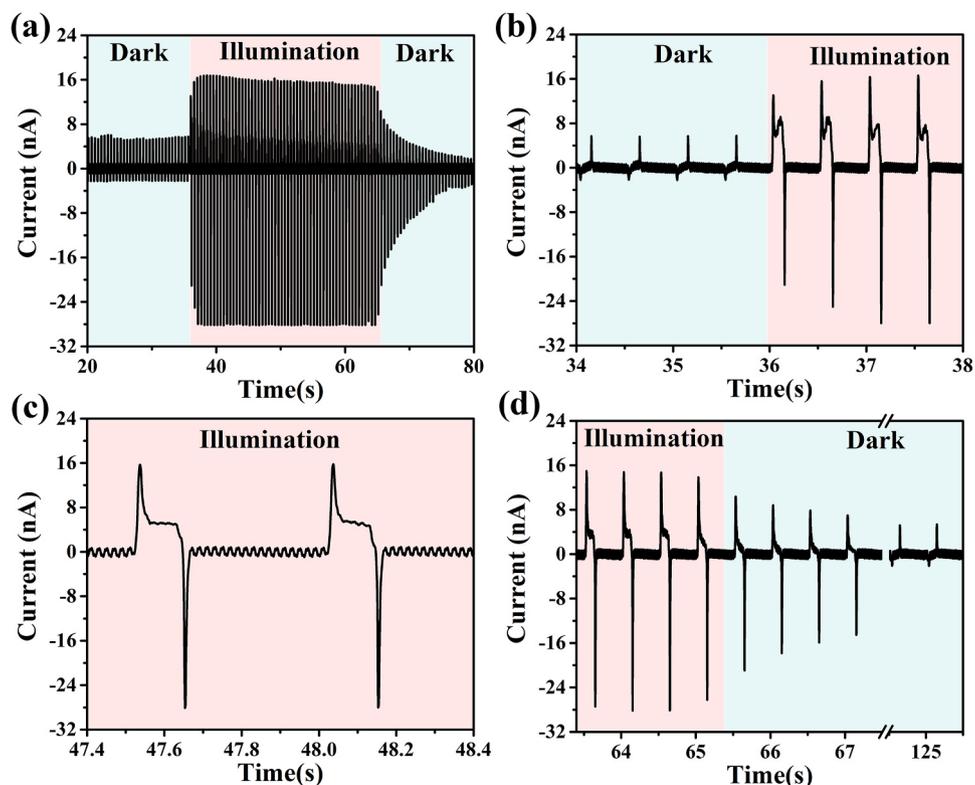

Fig. 3. The comparison and magnified details of the TENG in dark and under illumination. (a) The output performance of the TENG in dark and under illumination. The enlarged plot of the TENG corresponding to outputs at the moment of (b) light on, (c) continuous light illumination, and (d) light off, respectively.
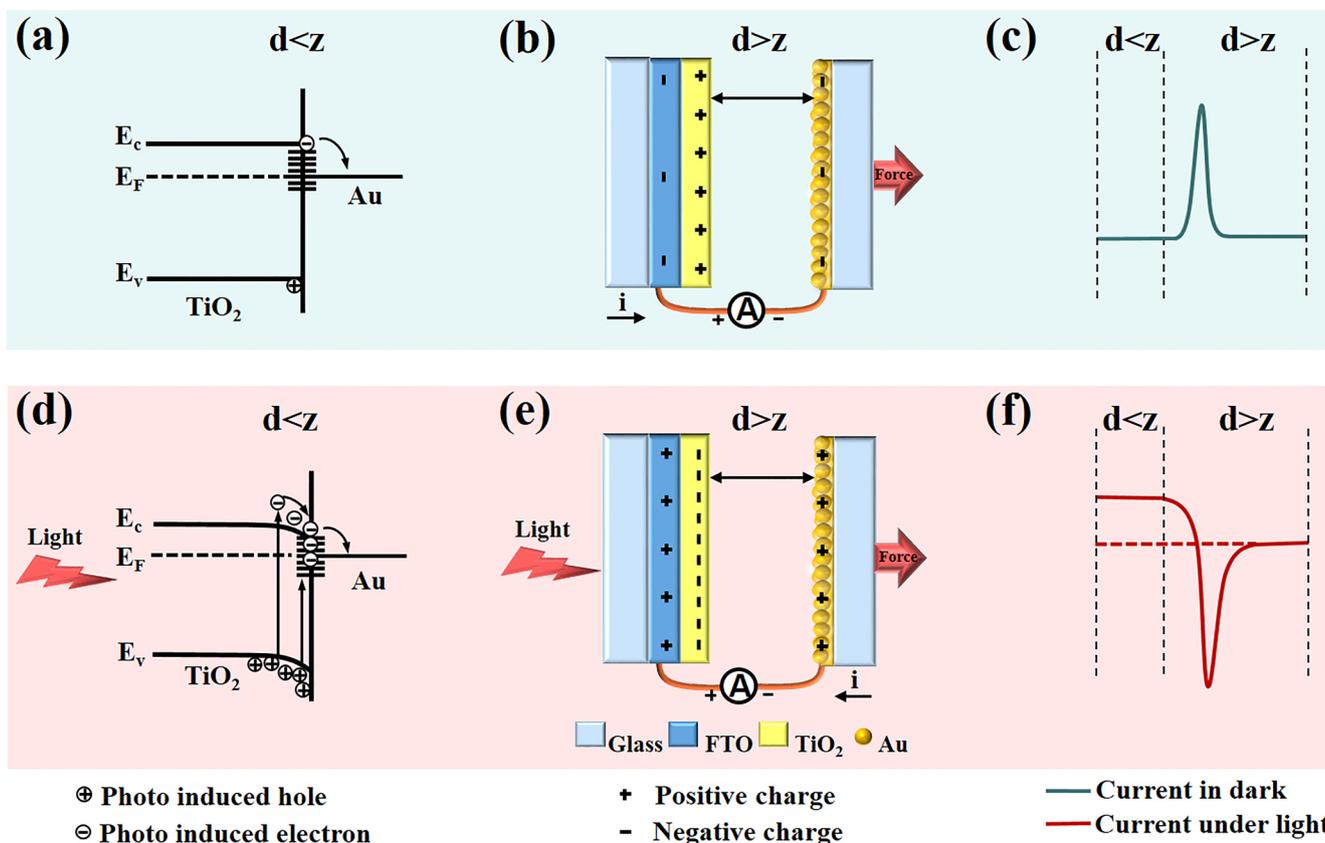
Fig. 4. The mechanism of TENG during the separation process in dark and under illumination. Energy band diagrams for the full contact between TiO_2 and Au when d < z, (a) in dark, (d) under illumination. Triboelectric polarity and distribution of surface triboelectric charges on TiO_2 and Au when d > z, (b) in dark, (e) under illumination. Schematic diagram of the current signal from the close contact of the two surfaces to the completely separation process, (c) in dark, (f) under illumination.
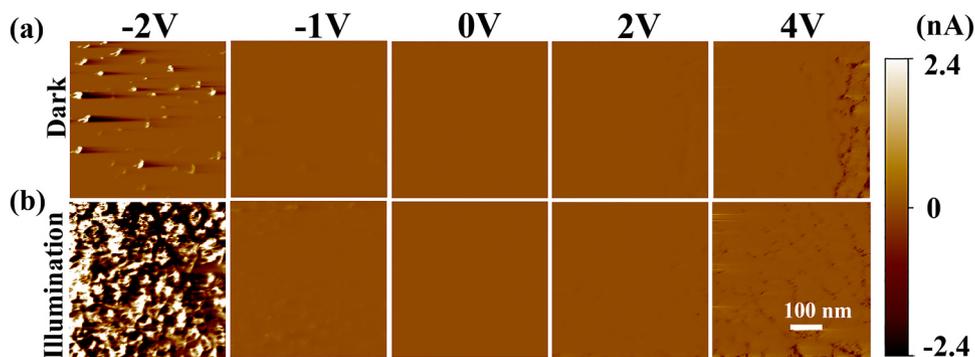

Fig. 5. Characterization of conductivity of TiO_2 films from -2–4 V by applying a bias voltage. (a) In dark, (b) under illumination.

under illumination. This conductivity improvement is also contributed to the output improvement [28]. The much larger current under illumination especially at negative bias confirms that photogenerated electrons are indeed trapped at the surface of TiO_2, as proposed in Fig. 4.

6. Conclusions

In summary, we designed a simple TENG based on TiO_2 and Au as the friction layers. Upon illumination, the positive current and the negative current output show the maximum of 2 and 12 times improvement. And because the special metal-semiconductor structure of FTO/TiO_2/Au is indeed a solar cell while in close contact, a photo-generated current plateau appears for this TENG device. By investigating the mechanism, we found that the main reason for the increase of TENG output under light illumination is the large number of photoelectrons accumulated on the surface of TiO_2, which change the relative triboelectric polarity of TiO_2 and Au, resulting in a markedly increase of current in the opposite direction. In addition, the improvement of photoconductivity of TiO_2 also contributes to the output current. By using metal and semiconductor as friction layer of a TENG device, this work demonstrates that both the polarity and the magnitude of the output current can be controlled by using surface trapped charges.

Acknowledgements

Notes

The authors declare no conflict of interest.

Appendix A. Supporting information

Supplementary data associated with this article can be found in the online version at doi:10.1016/j.nanoen.2019.01.019.

References

[1] F.-R. Fan, Z.-Q. Tian, Z.L. Wang, Flexible triboelectric generator, Nano Energy 1 (2012) 328–334.

[2] T.-C. Hou, Y. Yang, H. Zhang, J. Chen, L.-J. Chen, Z.L. Wang, Triboelectric nanogenerator built inside shoe insole for harvesting walking energy, Nano Energy 2 (2013) 856–862.

[3] Y. Su, X. Wen, G. Zhu, J. Yang, J. Chen, P. Bai, Z. Wu, Y. Jiang, Z.L. Wang, Hybrid triboelectric nanogenerator for harvesting water wave energy and as a self-powered distress signal emitter, Nano Energy 9 (2014) 186–195.

[4] Z.H. Lin, G. Zhu, Y.S. Zhou, Y. Yang, P. Bai, J. Chen, Z.L. Wang, A self-powered triboelectric nanosensor for mercury ion detection, Angew. Chem. Int. Ed. Engl. 52 (2013) 5065–5069.

[5] X. Pu, H. Guo, J. Chen, X. Wang, Y. Xi, C. Hu, Z.L. Wang, Eye motion triggered self-powered mechnosensational communication system using triboelectric nanogenerator, Sci. Adv. 3 (2017) (e1700694-e1700694).

[6] G. Zhu, C. Pan, W. Guo, C.Y. Chen, Y. Zhou, R. Yu, Z.L. Wang, Triboelectric-generator-driven pulse electrodeposition for micropatterning, Nano Lett. 12 (2012) 4960–4965.

[7] X.-S. Zhang, M.-D. Han, R.-X. Wang, R. Meng, F.-Y. Zhu, X.-M. Sun, W. Hu, W. Wang, Z.-H. Li, H.-X. Zhang, High-performance triboelectric nanogenerator with enhanced energy density based on single-step fluorocarbon plasma treatment, Nano Energy 4 (2014) 123–131.

[8] G. Zhu, Z.-H. Lin, Q. Jing, P. Bai, C. Pan, Y. Yang, Y. Zhou, Z.L. Wang, Toward large-scale energy harvesting by a nanoparticle-enhanced triboelectric nanogenerator, Nano Lett. 13 (2013) 847–853.

[9] G. Liu, H. Guo, L. Chen, X. Wang, D. Wei, C. Hu, Double-induced-mode integrated triboelectric nanogenerator based on spring steel to maximize space utilization, Nano Res. 9 (2016) 3355–3363.

[10] H. Guo, X. He, J. Zhong, Q. Zhong, Q. Leng, C. Hu, J. Chen, L. Tian, Y. Xi, J. Zhou, A nanogenerator for harvesting airflow energy and light energy, J. Mater. Chem. A 2 (2014) 2079–2087.

[11] Q. Tang, M.-H. Yeh, G. Liu, S. Li, J. Chen, Y. Bai, L. Feng, M. Lai, K.-C. Ho, H. Guo, C. Hu, Whirligig-inspired triboelectric nanogenerator with ultrahigh specific output as reliable portable instant power supply for personal health monitoring devices, Nano Energy 47 (2018) 74–80.

[12] X. Meng, Q. Cheng, X. Jiang, Z. Fang, X. Chen, S. Li, C. Li, C. Sun, W. Wang, Z.L. Wang, Triboelectric nanogenerator as a highly sensitive self-powered sensor for driver behavior monitoring, Nano Energy 51 (2018) 721–727.

[13] Z.H. Lin, Y.N. Xie, Y. Yang, S.H. Wang, G. Zhu, Z.L. Wang, Enhanced triboelectric nanogenerators and triboelectric nanosensor using chemically modified TiO$_2$ nanomaterials, ACS Nano 7 (2013) 4554–4560.

[14] Z.-H. Lin, G. Cheng, W. Wu, K.C. Pradel, Z.L. Wang, Dual-mode triboelectric nanogenerator for harvesting water energy and as a self-powered ethanol nanosensor, ACS Nano 8 (2014) 6440–6448.

[15] Z.H. Lin, G. Cheng, Y. Yang, Y.S. Zhou, S. Lee, Z.L. Wang, Triboelectric nanogenerator as an active UV photodetector, Adv. Funct. Mater. 24 (2014) 2810–2816.

[16] A.S. Uddin, U. Yaqoob, G.S. Chung, Improving the working efficiency of a triboelectric nanogenerator by the semimetallic PEDOT:PSS hole transport layer and its application in self-powered active acetylene gas sensing, ACS Appl. Mater. Interfaces 8 (2016) 30079–30089.

[17] Y.S. Zhou, Y. Liu, G. Zhu, Z.H. Lin, C. Pan, Q. Jing, Z.L. Wang, In situ quantitative study of nanoscale triboelectrification and patterning, Nano Lett. 13 (2013) 2771–2776.

[18] L. Su, Z.X. Zhao, H.Y. Li, J. Yuan, Z.L. Wang, G.Z. Cao, G. Zhu, High-performance organolead halide perovskite-based self-powered triboelectric photodetector, ACS Nano 9 (2015) 11310–11316.

[19] L. Su, Z. Zhao, H. Li, Y. Wang, S. Kuang, G. Cao, Z. Wang, G. Zhu, Photoinduced enhancement of a triboelectric nanogenerator based on an organolead halide perovskite, J. Mater. Chem. C 4 (2016) 10395–10399.

[20] B.U. Ye, S.Y. Lee, M. Jung, S.D. Sohn, H.J. Shin, M.H. Song, K.J. Choi, J.M. Baik, Photo-stimulated triboelectric generation, Nanoscale 9 (2017) 18597–18603.

[21] Z. Lin, X. Wang, J. Liu, Z. Tian, L. Dai, B. He, C. Han, Y. Wu, Z. Zeng, Z. Hu, On the role of localized surface plasmon resonance in UV–Vis light irradiated Au/TiO$_2$ photocatalysis systems: pros and cons, Nanoscale 7 (2015) 4114–4123.

[22] B. Bharti, S. Kumar, H.-N. Lee, R. Kumar, Formation of oxygen vacancies and Ti^{3+} state in TiO$_2$ thin film and enhanced optical properties by air plasma treatment, Sci. Rep. 6 (2016).

[23] G. Zhou, S. Duan, P. Li, B. Sun, B. Wu, Y. Yao, X. Yang, J. Han, J. Wu, G. Wang, L. Liao, C. Lin, W. Hu, C. Xu, D. Liu, T. Chen, L. Chen, A. Zhou, Q. Song, Coexistence of negative differential resistance and resistive switching memory at room temperature in TiO$_x$ modulated by moisture, Adv. Electron. Mater. 4 (2018).

[24] A.T. Raghavender, A.P. Samantilleke, P. Sa, B.G. Almeida, M.I. Vasilevskiy, N.H. Hong, Simple way to make anatase TiO$_2$ films on FTO glass for promising solar cells, Mater. Lett. 69 (2012) 59–62.

[25] Y.S. Zhou, S. Wang, Y. Yang, G. Zhu, S. Niu, Z.H. Lin, Y. Liu, Z.L. Wang, Manipulating nanoscale contact electrification by an applied electric field, Nano Lett. 14 (2014) 1567–1572.

[26] J. Bisquert, A. Zaban, P. Salvador, Analysis of the mechanisms of electron recombination in nanoporous TiO$_2$ dye-sensitized solar cells. Nonequilibrium steady-state statistics and interfacial electron transfer via surface states, J. Phys. Chem. B 106 (2002) 8774–8782.

[27] L. Jing, S. Li, S. Song, L. Xue, H. Fu, Investigation on the electron transfer between anatase and rutile in nano-sized TiO$_2$ by means of surface photovoltage technique and its effects on the photocatalytic activity, Sol. Energy Mater. Sol. Cells 92 (2008) 1030–1036.

[28] Y. Li, J.K. Cooper, W. Liu, C.M. Sutter-Fella, M. Amani, J.W. Beeman, A. Javey, J.W. Ager, Y. Liu, F.M. Toma, I.D. Sharp, Defective TiO$_2$ with high photoconductive gain for efficient and stable planar heterojunction perovskite solar cells, Nat. Commun. 7 (2016) 12446.
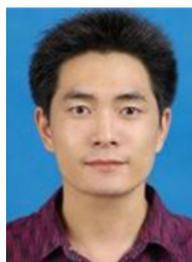
Juanjuan Han received her B.S. degree from Lanzhou University of Technology in 2016, and now she is pursuing the Master degree at Southwest University in professor Qunliang Song's group. Her research interests focus on triboelectric nanogenerators and self-powered photodetectors.

Xiude Yang received his master's degree from Guizhou Normal university, Guiyang, China in 2006. Currently, he is an associate professor in School of Physics and Electronic science, Zunyi normal college in china. Now, he is studying for his doctor's degree in Institute for Clean Energy & Advanced Materials (ICEAM), Southwest University, Chongqing, China. His research interests are renewable energy devices, such as nanogenerators for mechanical energy harvesting, solar cells, etc.

Liping Liao has received Bachelor's Degree from Beijing Institute of Graphic Communication in June 2014. So far, she is studying for a Master's Degree in Institute for Clean Energy & Advanced Materials of Southwest University and she is focusing on researches about perovskite solar cells.

Guangdong Zhou has received doctoral degree in Southwest University (China) in June 2018. Dr. Zhou is conducting his postdoctoral research in Southwest University during 2018.07–2020.07. His researches mainly focus on the memristor physical mechanism and memristor-based chip application in information storages, memory logic devices and bioinspired computing. His memristor-based research is supported by the Postdoctoral Program for Innovative Talent Support of Chongqing.

Gang Wang received his M.S degree from Southwest University in 2016, and now he is pursuing the Ph.D. degree at Southwest University. His research interest focuses on organic solar cells and perovskite solar cells.

Mbeng Elisabeth Reine Debora received her bachelor in INSTITUT UNIVETSITAIRE DE LA COTE in Cameroon in 2016. And she is pursuing her M.S. degree in Southwest University. Her research is based in policies related to renewable energy.

Cunyun Xu received his B.S. degree from Lanzhou University of Technology in 2016, and now he is pursuing the Master degree at Institute for Clean Energy & Advanced Materials of Southwest University. His research interest focuses on perovskite solar cells.

Qunliang Song is a physicist of Southwest University and received his doctoral degree from the Fudan University (China) in 2006. In 2008, Prof. Song was founded by the Lee kuan Yew Postdoctoral Fund and conducted his post-doctoral research in Nanyang Technological University. His research in organic solar cell was gradually shifted to perovskite solar cells, resistance switching memory devices and triboelectric nanogenerator. During the last 10 years, over 120 peer-reviewed papers were published.

Wei Hu received her B.S. degree from China West Normal University in 2016, and now she is pursuing the Master degree at Southwest University in professor Qunliang Song's group. Her research interest focuses on perovskite solar cells.